Photobiomodulation and photodynamic therapy-induced switching of autophagy and apoptosis in human dermal fibroblasts.

Viktoria Pevna[1], Denis Horvath[2], Georges Wagnieres[3] and Veronika Huntosova[2,*]

[1]Department of Biophysics, Institute of Physics, Faculty of Science, P.J. Safarik University in Kosice, Jesenna 5, 041 54 Kosice, Slovakia; viktoria.pevna@student.upjs.sk

[2]Center for Interdisciplinary Biosciences, Technology and innovation park, P.J. Safarik University in Kosice, Jesenna 5, 041 54 Kosice, Slovakia; denis.horvath@upjs.sk, veronika.huntosova@upjs.sk

[3]Laboratory for Functional and Metabolic Imaging, Institute of Physics, Swiss Federal Institute of Technology in Lausanne (EPFL), Station 3, Building PH, 1015 Lausanne, Switzerland; georges.wagnieres@epfl.ch

*****Correspondence: veronika.huntosova@upjs.sk

Abstract:

Nowadays, photobiomodulation (PBM) in combination with chemotherapy or other therapeutic approaches is an attractive adjuvant modality for cancer treatment. Targeted destruction of cancer cells is one of the main advantages of photodynamic therapy (PDT). We have shown in previous studies that the combination of PBM at 808 nm and hypericin-mediated PDT increases PDT efficacy in human glioblastoma cells U87 MG. The study presented here shows significant differences between U87 MG and non-cancerous human dermal fibroblasts (HDF) cells treated by PBM and PDT. This study focuses on mitochondria because PBM mainly affects these organelles. We demonstrated that an interplay between mitochondrial and autophagic proteins plays a crucial role in the response of HDF cells to PBM and PDT. Fluorescence microscopy, flow cytometry, and Western blot analysis were used to examine the autophagic profile of HDF cells after these treatments. An increase in ubiquitin, SQSTM1, LC3BII, and cytochrome c was accompanied by a decrease in M6PR, ATG16L1, and Opa1 in HDF cells exposed to PBM and PDT. Overall, we observed that the switching of autophagy and apoptosis is dose-dependent and also occurs independently of PBM in HDF cells after hypericin-mediated PDT. However, PBM might preferentially induce autophagy in noncancer cells, which might escape apoptosis under certain conditions.

Keywords: apoptosis, autophagy, human dermal fibroblast, photobiomodulation, photodynamic therapy, mitochondria, hypericin

1. Introduction

Photobiomodulation (PBM), in which metabolic signals are preferentially activated in mitochondria [1,2], has received considerable attention in recent decades. It has been reported that mitochondrial dynamics in response to PBM is controlled by several proteins: Mitofusin 2, Dynamin-related Protein 1, Cytochrome c, and Optic

Atrophy 1 (Opa1) [3,4]. The stimuli that trigger this activation are still unclear. However, research on PBM mechanisms has mainly focused on the role of cytochrome c oxidase [1,5].

Photodynamic therapy (PDT) combines photosensitizers, light, and oxygen to generate oxidative stress and destroy cancer cells by inducing apoptosis through mitochondrial signalling pathways [6]. Recently, the combination of PBM and photodynamic therapy (PDT) has been used in anticancer, antiviral, and antibacterial treatments [7–9].

Hypericin is an interesting molecule for cancer diagnosis and PDT [10,11], both *in vitro* and *in vivo* [11–15]. The main obstacle for this treatment is the hydrophobic nature of this molecule [16]. In general, the efficacy of PDT strongly depends on the active/therapeutic concentration of a photosensitizer, its localization, and, of course, the light dose used. To ensure high specificity in eliminating cancer cells, the concentration of the photosensitizer in healthy cells must be minimised.

In a previous study, we demonstrated a positive effect of PBM on hypericin-mediated PDT in cancer cells U87 MG [17]. Obviously, there is a question about the effect of the combination of PBM and PDT in non-cancerous cells. For this reason, HDF cells were used in the study presented here. HDF cells are also studied because they represent the important tissue layer exposed to PDT.

The present study focuses on mitochondria and autophagic proteins in HDF cells under PBM- and hypericin-induced combination treatment of PBM and PDT.

2. Material and methods

2.1. Cell cultures

Human dermal fibroblasts (HDF, 106-05a obtained from Cell, APPLICATIONS, Canada) were grown in RPMI 1640 (LM-R1638/500, biosera, Nuaille, France). U87 MG human glioma cells (Cells Lines Services, Eppelheim, Germany) were grown in DMEM (Dulbecco's modified Eagle medium, high glucose, GlutaMAX™, with pyruvate, Gibco-Invitrogen, Life Technologies Ltd., Paisley, UK). Cell culture media were supplemented with 10% FBS (foetal bovine serum, Gibco-Invitrogen, Life Technologies Ltd., Paisley, UK) and 1% (w/w) penicillin/streptomycin (Gibco-Invitrogen, Life Technologies Ltd., Paisley, UK). Cell cultures were purchased from Cells Lines Services, Eppelheim, Germany). Cultures were seeded in flasks or Petri dishes and grown in the dark under humidified atmosphere, 5% CO_2, and 37°C to 80% confluency.

2.2. Therapeutical protocols

Four therapeutic protocols (as illustrated in **Figure 1A**) were evaluated. Protocol (1): hypericin (Sigma-Aldrich, Germany) was administered to cells in the dark. After 3 hours, the medium containing hypericin was removed, replaced with fresh complete medium, and the cells were kept in the dark for 24 hours. Protocol (2): cells were treated with PBM immediately before administration of hypericin, and the protocol was

performed as in (1). Protocol (3): hypericin was administered to cells in the dark. After 3 hours, the medium containing hypericin was removed and replaced with fresh complete medium. Cells were treated with PDT and kept in the dark for 24 hours. Protocol (4): cells were treated with PBM immediately before hypericin administration, and the protocol was performed as in (3). All protocols were studied at the same time interval. PBM (808 ± 3 nm diode laser (MDL-III-808/1~2500 mW, Changchun New Industries Optoelectronics Tech. Co. Ltd., Changchun, China), 2 minutes, 1.8 J/cm^2, 15 mW/cm^2) was applied just before the administration of hypericin in the concentration range 100-500 nM. Hypericin was removed from the cell culture medium 3 hours before PDT (590 ± 10 nm light emitting diodes (homemade system), 2 minutes, 2 J/cm^2, 16.7 mW/cm^2).

The stock solution of hypericin was 2 mM in 100% dimethyl sulfoxide (DMSO, Sigma-Aldrich). Appropriate aliquots were added to cell culture media containing less than 0.025% DMSO (at 500 nM hypericin).

2.3. Cell metabolism assay

HDF and U87 MG cells were seeded in 24-well plates. Cells were treated according to the protocols shown in **Figure 1A**. Detection of cellular metabolism was performed according to the supplier's protocol and 24 hours after the treatments. In this assay, 3-(4,5-dimethylthiazol-2-yl)-2,5-diphenyltetrazolium bromide (MTT, Sigma-Aldrich, St. Louis, MO, USA) is converted to purple formazan, which is then dissolved in DMSO. Aliquots of 100 µl of the dissolved solutions were transferred to corresponding wells of 96-well plates and detected at 560 nm using a plate reader (GloMax TM-MultiDetection system with Instinct Software, Madison, WI, USA). These measurements were performed in triplicate. The mean values of 15 measurements were plotted in histograms. The error bars represent the standard deviations. Levels of significant differences were calculated using the one-way ANOVA test: *$p < 0.05$, **$p < 0.01$, *** $p < 0.001$.

2.4. Flow cytometric measurement of apoptosis and necrosis

HDF cells were treated according to the protocols in **Figure 1A**. Five hours after PDT, cells were harvested with trypsin/EDTA (ThermoFisher Scientific) and centrifuged at 600 rpm. Cell pellets were resuspended in Annexin V binding buffer (Mitenyi Biotec B.V. & Co. KG, Bergisch Gladbach, Germany) with AnnexinV/FITC (Mitenyi Biotec B.V. & Co. KG, Bergisch Gladbach, Germany). Propidium iodide (Mitenyi Biotec B.V. & Co. KG, Bergisch Gladbach, Germany) was added to the cell suspension immediately prior to detection by flow cytometer (MACSQuant® Analyzer, Miltenyi, Bergisch Gladbach, Germany) in the channels for FITC (B1) and PE-Vio770 (B4). These measurements were performed in duplicate.

2.5. Confocal fluorescence microscopy

HDF cells were grown in confocal petri dishes embedded with cover slide (SPL, Gyeonggi-do, Korea). Cells were grown for 24 hours in the presence of 10 µM rotenone (Sigma-Aldrich, Darmstadt, Germany) to induce mitochondrial damage. Mitochondria were observed in cells treated with these protocols 24 hours after treatment. Mitochondria were labeled with 5 µM Rhodamine 123 (Rh123, Sigma-Aldrich,

Darmstadt, Germany) for 15 minutes (Rhodamine 123 was excited at 488 nm and its emission was detected between 490 and 560 nm). Cell nuclei were labeled with 10 µg/mL Hoechst 33258 (ThermoFisher Scientific, Waltham, MA, USA) for 30 minutes (excitation at 405 nm and emission in the spectral range 450±40 nm). Lysosomes were labeled with 400 nM LysoTracker Blue (ThermoFisher Scientific) (excitation at 405 nm and emission in the spectral range 450±40 nm). Plasma membranes were stained with Cell Mask Orange (ThermoFisher Scientific) according to the supplier's protocol (excitation at 488 nm and emission in the spectral range >560 nm). Hypericin was detected in the spectral range >590 nm after excitation at 555 nm. The medium containing the fluorescent probes was replaced with fresh complete medium heated to 37°C prior to measurements. These measurements were performed in duplicate. Staining with all probes was performed both individually and as a cocktail. Spectral separation was adjusted according to separate color detection.

Giantin and LC3B were visualized in the cells by immunostaining. Cells were fixed with ice-cold (- 20 °C) acetone (Centralchem, Bratislava, Slovakia) for 5 minutes at – 20 °C and washed in ice-cold (4 °C) phosphate-buffered saline solution (PBS, Sigma-Aldrich, Darmstadt, Germany). Cells were blocked with 5 % bovine serum albumin (BSA, Sigma-Aldrich, Darmstadt, Germany) in PBS at room temperature (25 °C) for 1 hour. The primary antibodies were dissolved in 5 % BSA: anti-Giantin (1:300, ab80864, Abcam, Cambridge, UK) and LC3B (1:300, ab221794, Abcam, Cambridge, UK) and incubated with the cells for 1 hour at room temperature or overnight at 4 °C. After incubation, cells were washed with ice-cold PBS. The secondary antibody conjugated with AlexaFluor 488 (1:1000, ab150077, Abcam, Cambridge, UK) were diluted in 1 % BSA and applied to the cells for 1 hour at room temperature. Fluorescence of AlexaFluor 488 was detected at 488 nm excitation and emission in the spectral range 490 - 530 nm. Mitochondria were stained with MitoTracker Orange CMTM/Ros (ThermoFisher Scientific, Waltham, MA, USA) for 15 min before fixation with acetone (excitation at 555 nm and emission in the spectral range > 560 nm). After fixation, nuclei were labeled with 10 µg/mL Hoechst 33258 (ThermoFisher Scientific, Waltham, MA, USA) for 5 minutes (excitation at 405 nm and emission in the spectral range 450±40 nm).

Fluorescence images were acquired using a confocal fluorescence microscope system (LSM 700, Zeiss, Oberkochen, Germany), a 40X water immersion objective (NA 1.2, Zeiss), and a CCD camera (AxioCam HRm, Zeiss). Fluorescence images were analyzed using Zen 2011 software (Zeiss). These measurements were performed in duplicate.

The fluorescence intensities of Rhodamine 123 and the size/number of organelles spreading in the areas detected by Giantin and LC3B were analyzed using ImageJ software [18].

2.6. Western blot assay

HDF and U87 MG cells were lysed at a density of 10^6 and homogenized in radioimmunoprecipitation buffer (RIPA) (150 mM sodium chloride, 1 % Triton X-100, 0.5 % sodium deoxycholate, 0.1 % sodium dodecyl sulfate, 50 mM Tris, pH 8; all chemicals were purchased from Sigma-Aldrich, Darmstadt, Germany) with the inhibitor

cocktail (2 × 1:100, Halt™ Protease & Phosphatase Inhibitor Cocktail, ThermoFisher Scientific, Waltham, MA, USA). Whole lysates (120 µg total protein amount) were diluted to 60 µg of final protein in 2x Laemmli buffer (Sigma-Aldrich, Darmstadt, Germany), loaded onto 7% or 15 % polyacrylamide gels, and subjected to electrophoresis. Proteins were transferred to a nitrocellulose membrane (0.45 µm; SERVA; Heidelberg, Germany). Hypericin was used at a concentration of 200 nM.

Immunodetection was performed using the Western Breeze Chromogenic Kit (ThermoFisher Scientific, Waltham, MA, USA). Proteins in the membrane were blocked with 5 % BSA for 1 hour at room temperature, washed, and then incubated overnight at 4 °C with primary antibodies: autophagy analysis (ATG16L1, SQSTM1, LC3B, Ubiquitin, M6PR) antibody sampler panel (ab269811, Abcam, Cambridge, UK), cytochrome c apoptosis WB antibody cocktail (ab110415, Abcam, Cambridge, UK) and anti-GAPDH (1:1000, ab181602, Abcam, Cambridge, UK) was determined as the housing protein. For protein visualization, secondary antibodies from the Western Breeze Chromogenic Kit were used to detect the primary rabbit and mouse antibodies. Analysis of the optical densities (O.D.) of proteins in the membrane was performed using ImageJ software. The normalized O.D. values shown in the histograms are the mean values of 3 measurements. The error bars represent the standard deviations.

2.7. Estimation of index of the treatment efficiency

We quantitatively assessed the therapeutic efficacy based on a complete set of experimental data. We claim to characterize how hypericin dose affects treatment outcomes under PBM, PDT, and PBM+PDT conditions. Specifically, we propose an indicator of therapeutic efficiency I_{MD} formulated as follows

$$I_{MD} = \ln (M_{45} / M_{23}) - \ln (D_{45} / D_{23}) = \ln [(M_{45} / D_{45}) / (M_{23} / D_{23})].$$

This indicator is designed to quantitatively reflect changes relative to a baseline. In this formula, M_{45} represents the average metabolic activity as the arithmetic mean of a pair of metabolic activities observed for two concentrations of hypericin (400 and 500 nM). The interest of this pairwise averaging is linked to the smoothing of fluctuations. When lower hypericin concentrations are considered, the value of M_{23} is the arithmetic mean of the metabolic activities determined at hypericin concentrations of 200 and 300 nM. Similarly, the average reference values of metabolic activity D_{45} and D_{23} are introduced, corresponding to the experiments performed in the dark. The logarithm ensures that if the ratio of, for example M_{45} / M_{23} is equal to one, this means that no change has occurred and the contribution to I_{MD} is zero. All of the above quantifications of M_{45}, M_{23}, D_{45}, and D_{23} were performed specifically for the PBM, PDT, and PBM+PDT groups. I_{MD} was calculated separately for non-neoplastic HDF and U87 MG neoplastic cells. The original data projected onto the six I_{MD} variants were then statistically processed and plotted in **Figure 1D** using the R package ‘vioplot’ and density estimation. Differences were visually apparent, but were further augmented by appropriate hypothesis tests for differences in treatment efficacy. **Table 1** provides an overview of these results.

Initial inspection of the data and detection of differences is followed by quantification, i.e., calculation of test statistics (also referred to as calculated value)

(often simply referred to as t-value in the case of Student's t-test and F-value in the case of ANOVA). They are calculated by loading the data into a statistical test procedure. The critical difference, however, is that in the case of the Student's t-test, the calculated t-value is the ratio between the difference between the means and the standard error, whereas the resulting F-value in the case of ANOVA is the ratio between the between-group variability and the within-group variability of the observations.

The one-way method ANOVA is used to find statistical evidence of inconsistencies or differences between the means of the selected group for specific conditions. However, the one-way method ANOVA assumes that each group originates from an approximately normal distribution and that the variability within groups is approximately constant, which may not be the case for the inputs I_{MD}. As shown in **Table 1**, the ANOVA is controversial in the two examples examined, where the Shapiro-Wilk test indicated a rejection of the Gaussianity of I_{MD}.

3. Results

3.1. Hypericin-mediated PDT induces apoptosis in HDF cells

The metabolic activity of cells determined by the MTT assay often reflects the viability and activity of mitochondria. **Figure 1B** shows the results of the MTT assay in HDF cells treated with PBM, PDT, and PBM+PDT. The response of cells is concentration dependent, but the efficacy of PDT did not reduce the metabolic activity of HDF cells below 50%. In comparison, the response of U87 MG to the same treatments was much stronger (**Figure 1C**). PDT significantly reduced the metabolic activity of cells below 50%. PBM enhanced the PDT effect in both cell lines. With the aim of avoiding the phototoxicity of HDF and maintaining the phototoxicity of U87 MG cells, we identified 200 nM hypericin as the most interesting concentration in our study. To better illustrate the comparison between HDF and U87MG cells, we estimated indicators of therapeutic efficiency in Figure 1D. The Welch two sample t-test, one-way ANOVA and Shapiro-Wilk tests of normality (see **Table 1**) revealed more significant effects in U87 MG than in HDF. In addition, significant differences were found between U87 MG and HDF cells under the PBM+PDT protocol.

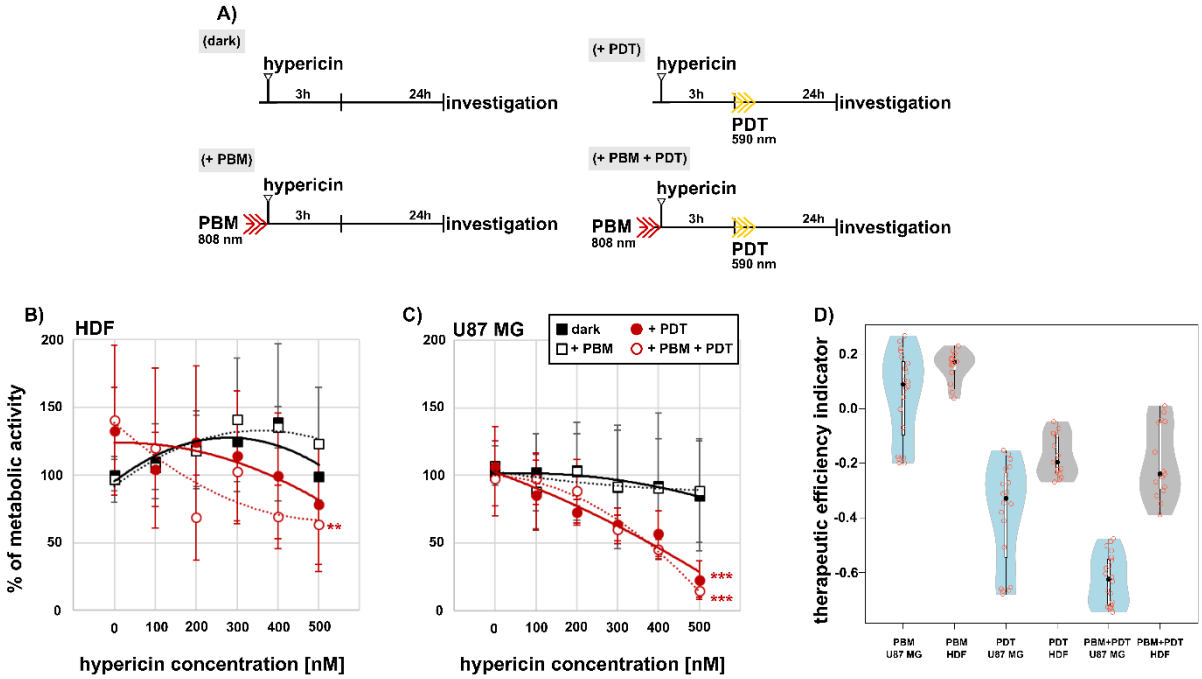

Figure 1: Metabolic activity of B) HDF and C) U87 MG cells treated with PDT (2 J/cm^2 at 590 nm) and PBM (1.8 J/cm^2 at 808 nm) using defined protocols as shown in A). The hypericin concentrations applied were 100, 200, 300, 400, and 500 nM. The level of significant differences (with respect to control) was determined using the one-way method ANOVA: **p < 0.01 and ***p < 0.001. D) Indicator of therapeutic efficiency for HDF (gray) and U87 MG cells (blue).

Table 1: Results illustrating the significant differences between protocols in U87MG and HDF cells determined with Welch two sample t-test, one-way ANOVA and Shapiro-Wilk tests of normality.

	Welch two sample t-test		**One-way ANOVA test**	
Pair of samples	t	p	F	Pr(>F)
$PBM_{U87\ MG}$~PBM_{HDF}	-2.72	1.14e-2 **	51.84	1.09e-5 ***
$PDT_{U87\ MG}$~PDT_{HDF}	-4.52	1.11e-4 ***	443.6	1.98e-11 ***
$PBM+PDT_{U87\ MG}$~$PBM+PDT_{HDF}$	-10.72	1.54e-10 ***	23.01	3.49e-4 ***
$PBM_{U87\ MG}$~$PDT_{U87\ MG}$	7.79	2.45e-9 ***	829.4	2.0e-16 ***
$PDT_{U87\ MG}$~$PBM+PDT_{U87\ MG}$	5.21	1.60e-5 ***	53.6	8.46e-7 ***
PBM_{HDF}~PDT_{HDF}	13.21	5.96e-13 ***	30.23	1.37e-4 ***
PDT_{HDF}~$PBM+PDT_{HDF}$	0.56	5.81e-1	52.09	6.78e-6 ***
	Shapiro-Wilk tests of normality			
sample	normality	W	p	
$PBM_{U87\ MG}$	rejected	0.890	0.027	
$PDT_{U87\ MG}$	rejected	0.863	0.008	
$PBM+PDT_{U87\ MG}$	-	0.910	0.065	
PBM_{HDF}	-	0.891	0.085	
PDT_{HDF}	-	0.896	0.084	
$PBM+PDT_{HDF}$	-	0.903	0.105	

AnnexinV/FITC and propidium iodide staining successfully indicated late apoptosis in more than 50% of the PDT-treated HDF cell population (**Figure 2**). The effect of PBM on PDT was not demonstrated by this method. However, the distribution of hypericin-loaded cell population was slightly different in HDF cells after PBM.

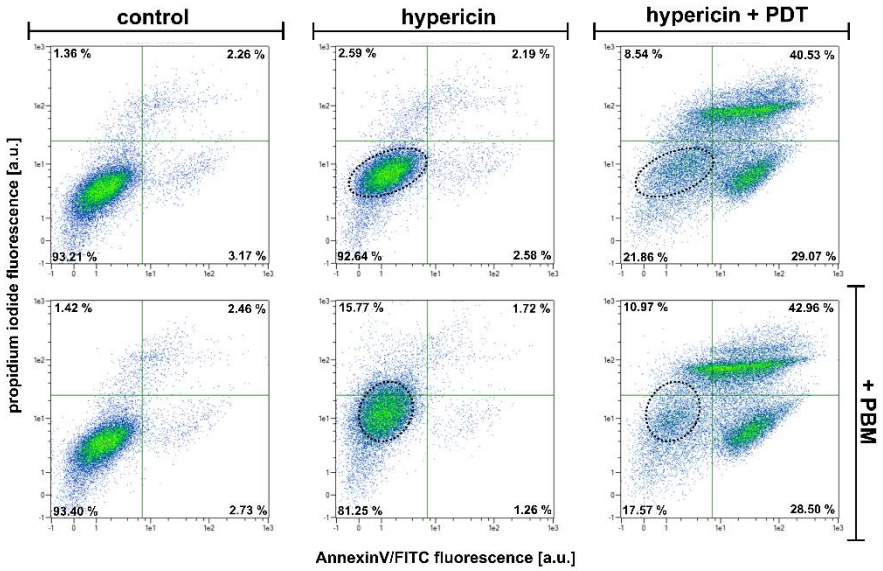

Figure 2: Apoptosis/necrosis assay based on AnnexinV/FITC and propidium iodide staining of HDF cells cultured according to the protocols shown in **Figure 1C** but detected 5 hours after PDT (2 J/cm^2 at 590 nm) instead of 24 hours. Cells treated with PBM (1.8 J/cm^2 at 808 nm) are in the second row. The number of cells is color coded from blue (minima) to red (maxima). The concentration of 200 nM hypericin was maintained for this study. Populations of hypericin-loaded cells were highlighted by black circular areas.

3.2. Mitochondrial changes in HDF cells after PDT

Morphological changes in HDF cells were detected by confocal fluorescence microscopy at the suborganelle level. Plasma membranes were labeled with Cell Mask Orange (red color in **Figure 3**), and live mitochondria were fluorescently identified with Rhodamine 123 (green color in **Figure 3**). The fluorescence of Rhodamine 123 is sensitive to mitochondrial membrane potential. While the intensity increased in hypericin-treated cells (**Figures 3B and 3F**), PDT of these cells resulted in a decrease in mitochondrial membrane potential and a significant decrease in Rhodamine 123 fluorescence intensity (**Figures 3C and 3F**). Interestingly, a significant decrease in fluorescence intensity was observed in HDF cells after the combination of PBM and PDT (**Figures 3D and 3F**).

The morphology of cell mitochondria treated with PDT was compared with mitochondria exposed to 10 μM rotenone (**Figure 3E**). Rotenone, an inhibitor of complex I of the respiratory chain, resulted in a decrease in Rhodamine 123 fluorescence and a change in mitochondrial morphology (**Figures 3E, F and I**). The tubular mitochondrial network was fragmented, and some mitochondria were curled (**Figure 3I**). This was not observed in cells after PDT, even when PBM and PDT were combined.

Cytoskeleton-like structures were observed after PDT that were colocalized with the cell mask. The spherical structures identified with the cell mask in the perinuclear regions of HDF cells transformed into fused complexed structures indicated by white arrows in **Figure 3H**. Note that hypericin fluorescence can be partially detected in the same fluorescence detection window as Cell Mask Orange. The blue color in **Figure 3**

belongs to Lysotracker Blue, which is localized in the lysosomes of HDF cells. Lysosome destruction and release of Lysotracker Blue were observed after PDT in **Figures 3C and 3D**.

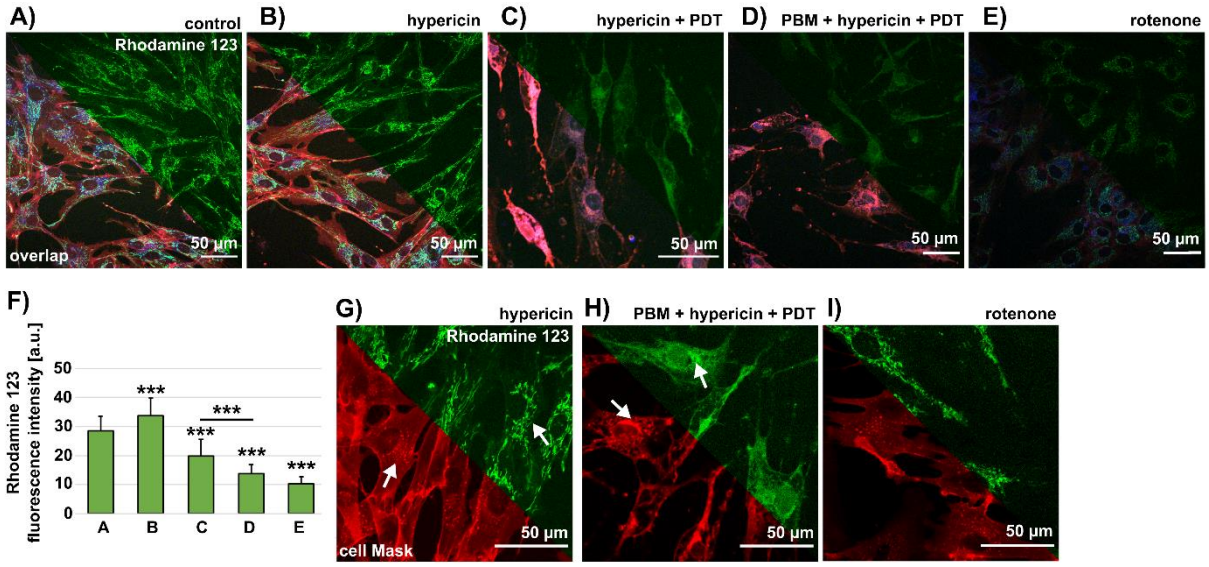

Figure 3: Fluorescence images of vital mitochondria in HDF cells stained with Rhodamine 123 (green): A) untreated control, B) 200 nM hypericin (protocol (1)), C) PDT (protocol (3)), D) PBM+PDT (protocol (4)), and E) 10 µM rotenone for 24 hours. The fluorescence intensity of Rhodamine 123 was evaluated ($n > 20$) and plotted in F). One-way test ANOVA was used to determine the level of significant differences: ***$p < 0.001$. The fluorescence intensities of Rhodamine 123 were increased in G-I) to better visualize the subcellular structures. Cell Mask Orange was applied to stain plasma membrane (red) and LysoTracker Blue was applied to the lysosomes (blue). White arrows indicate vesicular structures in the perinuclear regions.

Cells were stained with fluorescent immunostaining against Giantin (green color in **Figure 4**), which is localized in the membranes of the Golgi complex, to identify the origin of the vesicular clusters found in the perinuclear regions after PDT. The structure of Golgi cisternae in HDF cells subjected to different treatments is shown in **Figure 4**. While well-defined cisternae were seen in control cells and cells treated with hypericin, fragmentation of cisternae was observed in cells treated with rotenone (**Figure 4E**). Interestingly, the Golgi complex was not fragmented in the cells after PDT (**Figures 4C and 4D**). In contrast, firmly adherent objects in the form of clusters were found in these cells.

A change in the distribution of Golgi cisternae after PDT was also detected when the size of Giantin objects was analyzed by measuring the propagation distances from the nucleus to the plasma membrane (**Figure 4F**). In cells exposed to rotenone, large distances were observed in the spreading of Giantin. The tight binding of mitochondria (red color in **Figure 4**) to the Golgi complex is evident from colocalization (yellow color). MitoTracker Orange is bound to mitochondria in fixed cells by the formation of disulfide bonds. The tubular network is more evident in PBM and PDT cells (**Figure 4D**) than in cells treated with PDT alone (**Figure 4C**).

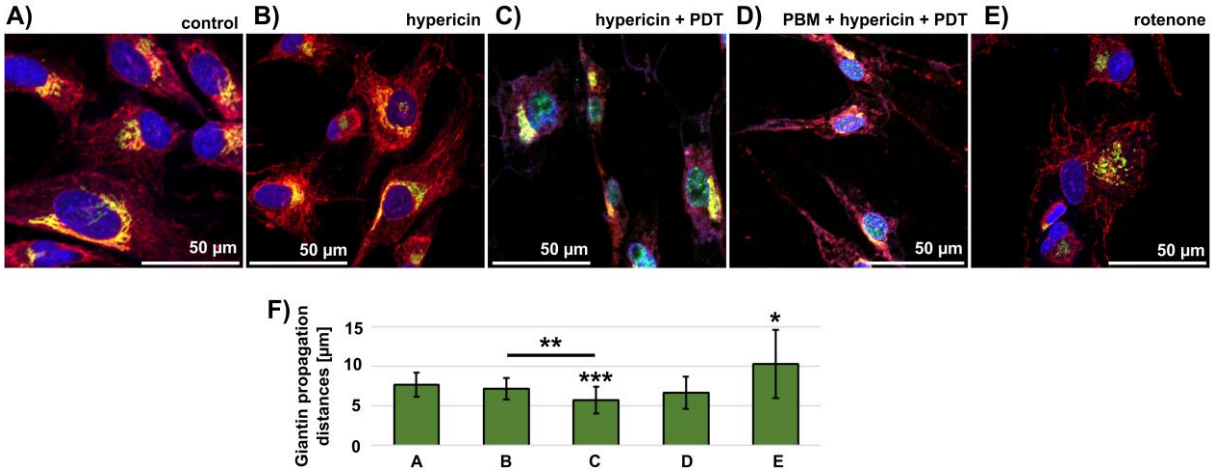

Figure 4: Fluorescence images of immunostained HDF cells with anti-Giantin and AlexaFluor 488 (green) and MitoTracker Orange (red, stained before acetone fixation): A) untreated control, B) 200 nM hypericin, C) PDT, D) PBM+PDT, and E) 10 µM rotenone. Hoechst was used to counterstain the nuclei (blue). F) The distances of Giantin spread from the nucleus to the plasma membrane were measured and plotted in histograms as Giantin propagation distances in µm (n > 16). One-way test ANOVA was used to determine the level of significant differences: *p < 0.05, **p < 0.01, and ***p < 0.001.

3.3. Autophagy in HDF cells is induced by PDT

The distribution of LC3B, an autophagic marker, in HDF cells was observed by confocal fluorescence microscopy in the immunostained cells. The granular structures loaded with LC3B were found in HDF cells without treatment (**Figure 5A**). The distribution and number of structures increased with the concentration of hypericin administered to HDF cells in the dark (**Figures 5B and 5C**). After PDT induced by 200 nM hypericin, more LC3B structures were found (**Figure 5D**), which further increased when BPM and PDT were combined (**Figure 5F**). Fewer LC3B structures were found in cells after PDT induced by 500 nM hypericin (**Figures 5E, G, and H**). However, significant changes in morphology related to the induction of cell death were observed in these cells, especially the deformation of the cell nuclei.

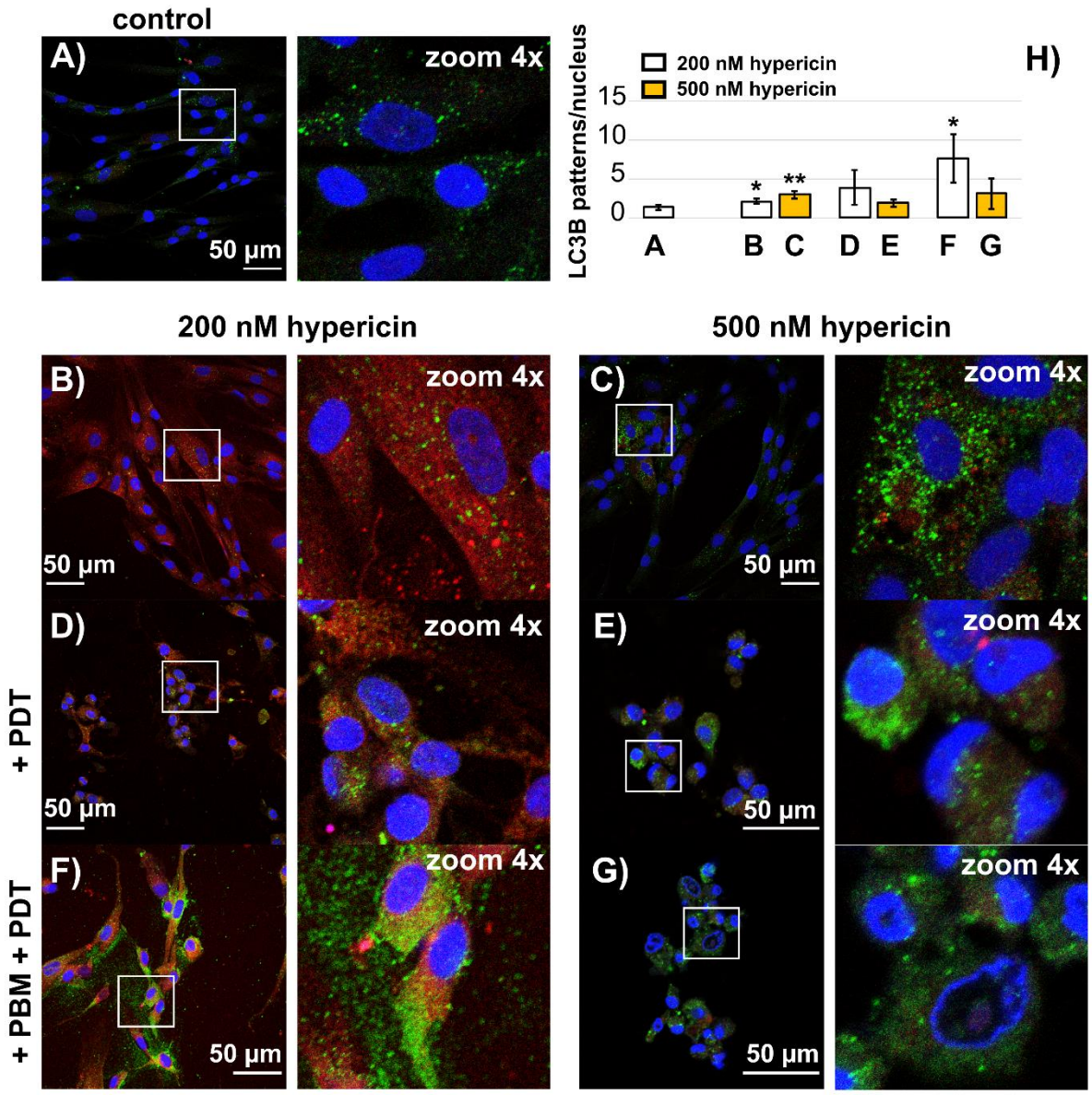

Figure 5: Fluorescence images of immunostained HDF cells with anti-LC3B and AlexaFluor 488 (green): A) untreated control, B) 200 nM hypericin, D) + PDT, F) + PBM+PDT and C) 500 nM hypericin, E) + PDT, G) + PBM+PDT. Hoechst was used to counterstain the nuclei (blue). The red fluorescence corresponds to hypericin. H) LC3B structures were counted and normalized per cell number (n > 30). One-way test ANOVA was used to determine the level of significant differences: *p < 0.05 and **p < 0.01.

Protein levels of autophagic proteins were examined in HDF and U87 MG cells subjected to selected treatments. **Figure 6** shows the results of Western blot analysis of mannose-6-phosphate receptor (M6PR, marker for lysosomal membranes), autophagy related 16 like 1 (ATG16L1, phagophore and recycling endosomes), sequestosome 1 (SQSTM1, marker for autophagy degradation), and LC3B (marker for autophagosomes) in HDF and U87 MG. Significant differences were found mainly in protein levels in cells subjected to PDT. While M6PR and ATG16L1 decreased in both cell lines after PDT, a significant increase in LC3BII levels was observed. SQTM1 levels increased in HDF cells and were not significantly changed in U87 MG cells,

except for PDT (SQTM1 level slightly decreased). LC3BI level increased in HDF cells with PBM and hypericin+PBM.

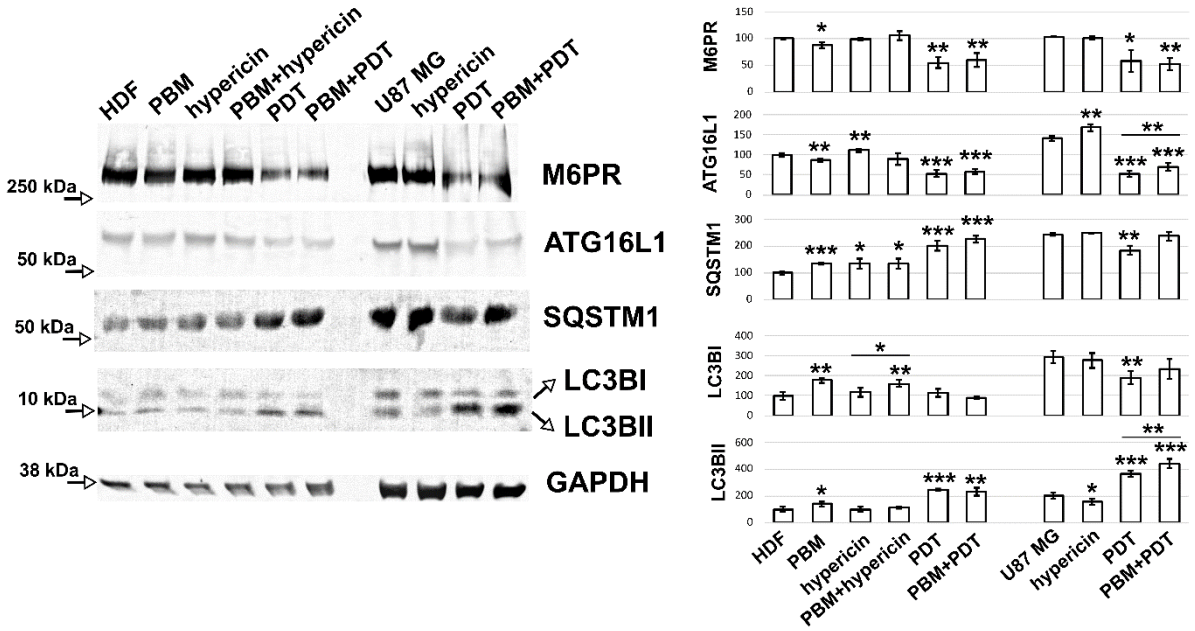

Figure 6: Autophagic proteins levels in HDF and U87 MG cells subjected to PBM, 200 nM hypericin and PDT according to protocols denoted in Figure 1C. Histograms represent mean Western blot densities normalized to GAPDH, a housing protein. A One-way test ANOVA was used to determine the level of significant differences: *$p < 0.05$, **$p < 0.01$ and ***$p < 0.001$.

3.4. Mitochondrial protein levels change in HDF cells after PBM and PDT

Protein levels of mitochondrial proteins were detected in HDF and U87 MG cells. Western blot analysis of CV α, PDH E1 α, and cytochrome c is shown in **Figure 7**. Significant increases in of PDH E1 α and cytochrome c levels were observed in HDF cells subjected to all the treatments examined. However, the most significant increase in of cytochrome c levels was observed in the PDT groups. The opposite effect was observed in U87 MG cells (**Figure 7**). The CV α levels decreased slightly in both PDT groups (PDT and PBM+PDT) in HDF cells, but in PDT only in U87 MG cells.

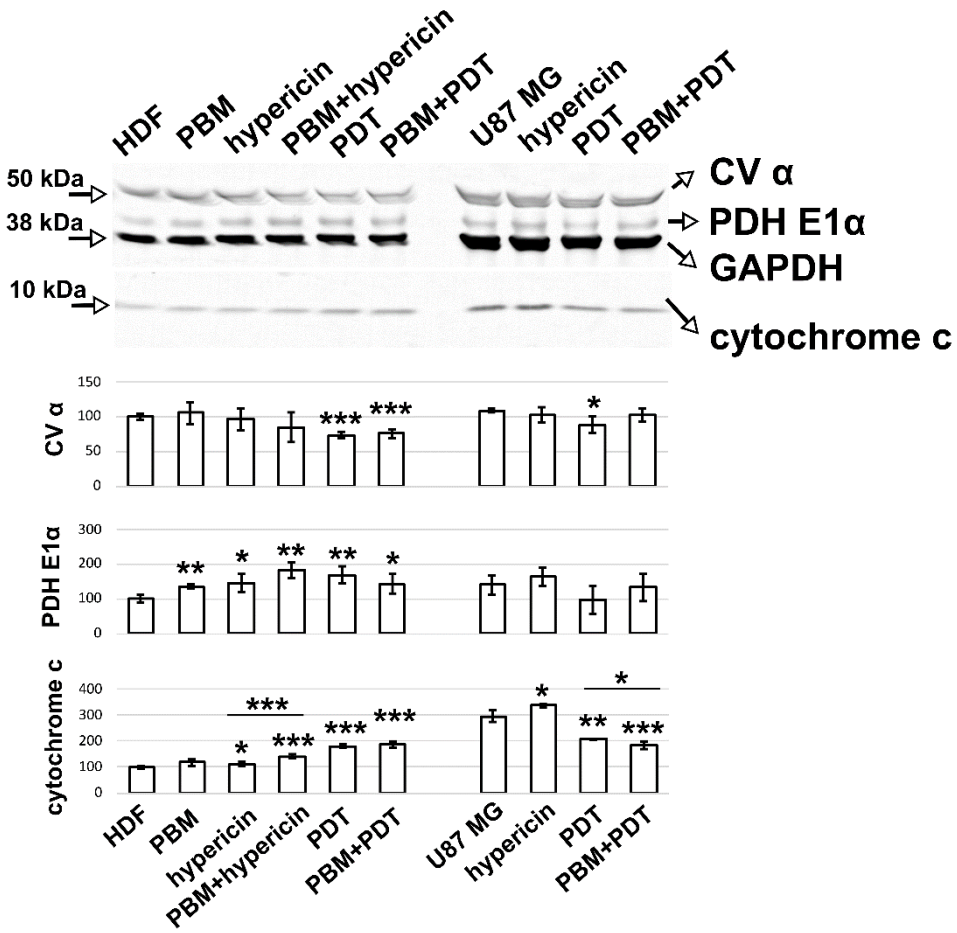

Figure 7: Mitochondrial protein levels in HDF and U87 MG cells subjected to PBM, 200 nM hypericin and PDT according to protocols denoted in Figure 1C. Histograms represent mean Western blot densities normalized to GAPDH, a housing protein. A One-way test ANOVA was used to determine the level of significant differences: *p < 0.05, **p < 0.01 and ***p < 0.001.

Ubiquitin and Opa1 protein levels were analysed in HDF cells only. Western blot analysis of HDF cells exposed to PBM, hypericin, PBM+hypericin, PDT, and PBM+PDT is shown in **Figure 8**. Ubiquitin levels in HDF cells increased with all treatments, but the most pronounced effect was observed after PDT and PBM+PDT. It should be noted that PBM caused an increase in Ubiquitin levels in HDF with and without hypericin treatment. In contrast, a reduction in Opa1 was observed in HDF cells after PDT and PBM+PDT.

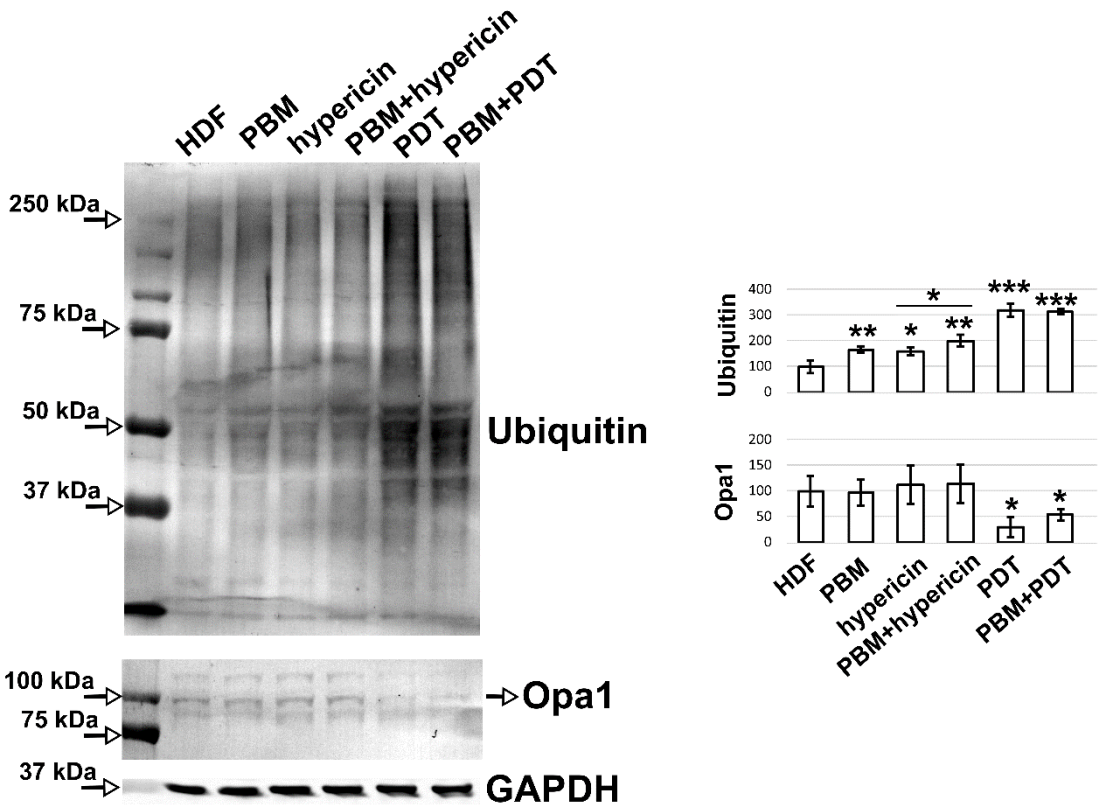

Figure 8: Ubiquitin and Opa1 proteins levels in HDF cells subjected to PBM, 200 nM hypericin and PDT according to protocols denoted in Figure 1C. Histograms represent mean Western blot densities normalized to GAPDH, a housing protein. A One-way test ANOVA was used to determine the level of significant differences: *p < 0.05, **p < 0.01 and ***p < 0.001. Protein standard was loaded in the first line.

4. Discussion

In this study, the metabolic activity assay (which is often used as a cell viability assay) was used to determine a critical hypericin concentration that inhibited the metabolic activity of HDF cells above 50% and of U87 MG cells below 50% after PDT. Hypericin at a concentration of 500 nM was hypothesised to cause significant photodamage in both cell types. In contrast, a hypericin concentration of 200 nM only slightly affects the metabolic activity of HDF cells after PDT, but may lead to a significant inhibition of the metabolic activity of U87 MG cells. In both groups studied, a substantial number of apoptotic positive HDF cells were detected by flow cytometry 5 hours after PDT and PBM+PDT. The apoptosis/necrosis profiles of HDF cells were drastically different from those observed in our previous study of U87 MG cells under the same conditions. It is difficult to accurately determine the PDT efficacy rate base on this measurement. However, nearly 30% of cells are early apoptotic (positive for annexinV/FITC and negative for propidium iodide) and 40% are late apoptotic (positive for annexinV/FITC and propidium iodide). Oxidative stress in these populations increases and, consequently, cell defence against processes related to the reduction of reactive oxygen species production increases as well. The rapid response of cells

could lead to reparative processes that would allow cells to escape the death machinery in later hours (24 hours after PDT).

The mitochondrial membrane potential measured in the present study with rhodamine123 decreased after PDT in HDF cells. This destabilisation of mitochondrial membrane potential suggests the generation of oxidative stress by PDT [19]. Interestingly, cells exposed to PBM+PDT showed a similar decrease in rhodamine123 fluorescence as rotenone, an inhibitor of mitochondrial respiration. However, mitochondrial morphology after PDT and PBM+PDT differed from that of rotenone-treated cells. The remaining mitochondria formed a large network that was not as abundantly branched as in rotenone-treated cells. Moreover, the Golgi complex remained tightly assembled in HDF cells after PDT and PBM+PDT. In HDF cells exposed to rotenone, massive degradation of the Golgi complex was observed. We can assume that the oxidative stress induced in HDF cells mobilised mitochondria to reduce the fatal effect of PDT [20]. Most proteins undergo their maturation in the Golgi apparatus [21], such as protein kinases. For this reason, the stability of the Golgi apparatus is very important for cell viability and further differentiation [22]. With regard to the assembly of the Golgi complex in HDF, it can be assumed that the cells are able to enhance the force to stimulate the defence against oxidative stress. For comparison, fragmentation of the cisternae of the Golgi apparatus was observed in U87 MG cells after hypericin-mediated PDT [23]. The explanation for these observations could be the intracellular hypericin concentration, which is presumably lower in HDF cells than in U87 MG cells.

As mentioned earlier, PDT and PBM+PDT resulted in photodestruction of mitochondria in HDF cells. In general, damaged mitochondria in cells are eliminated by the process of mitophagy, in which the damaged mitochondria are either repaired or eliminated and replaced by new functional mitochondria [24–26]. The mechanism by which this process occurs is associated with autophagy, in which lysosomal vesicles play an important role. Lysosomes cooperate with the degradation of mitochondria in the newly formed autophagosome structure [27,28]. The formation of this structure can be monitored by proteins involved in autophagosome formation. LC3B protein is part of the autophagosomal membrane. The increase of LC3BII in HDF cells after PDT indicates a delay in autophagosome degradation. The balance of oxidative stress in this condition is important for the further fate of the cell. This was the case in HDF cells exposed to 500 nM hypericin-mediated PDT (**Figure 5**). We can also assume that PBM induces low oxidative stress in cells. In contrast to PDT, the increase in LC3BI in HDF cells suggests an autophagy repair process after PBM and PBM+hypericin. This may be supported by the results of Western blot analysis, in which lysosomal membrane-associated M6PR and ATG16L1 were still present in these cells. However, the levels of these proteins decreased in the cells after PDT, whereas SQSTM1 (which is associated with late autophagosome formation) and also ubiquitin increased. SQSTM1 is a ubiquitin-binding scaffold protein and serves as a link for the degradation of ubiquitinated proteins in lysosomes during autophagy [29]. Since an increase in both proteins was observed, a problem with autophagosome degradation after PDT may be expected. Considering the results obtained in our study, we proposed PBM, PBM+hypericin, and PBM+PDT action regimens in HDF cells (see **Figure 9**). The increase in cytochrome c and decrease in Opa1 levels suggest that the fission and

fusion of the mitochondrial network is rebalanced by the generation of reactive oxygen species [30], a mechanism that is disrupted after PDT.

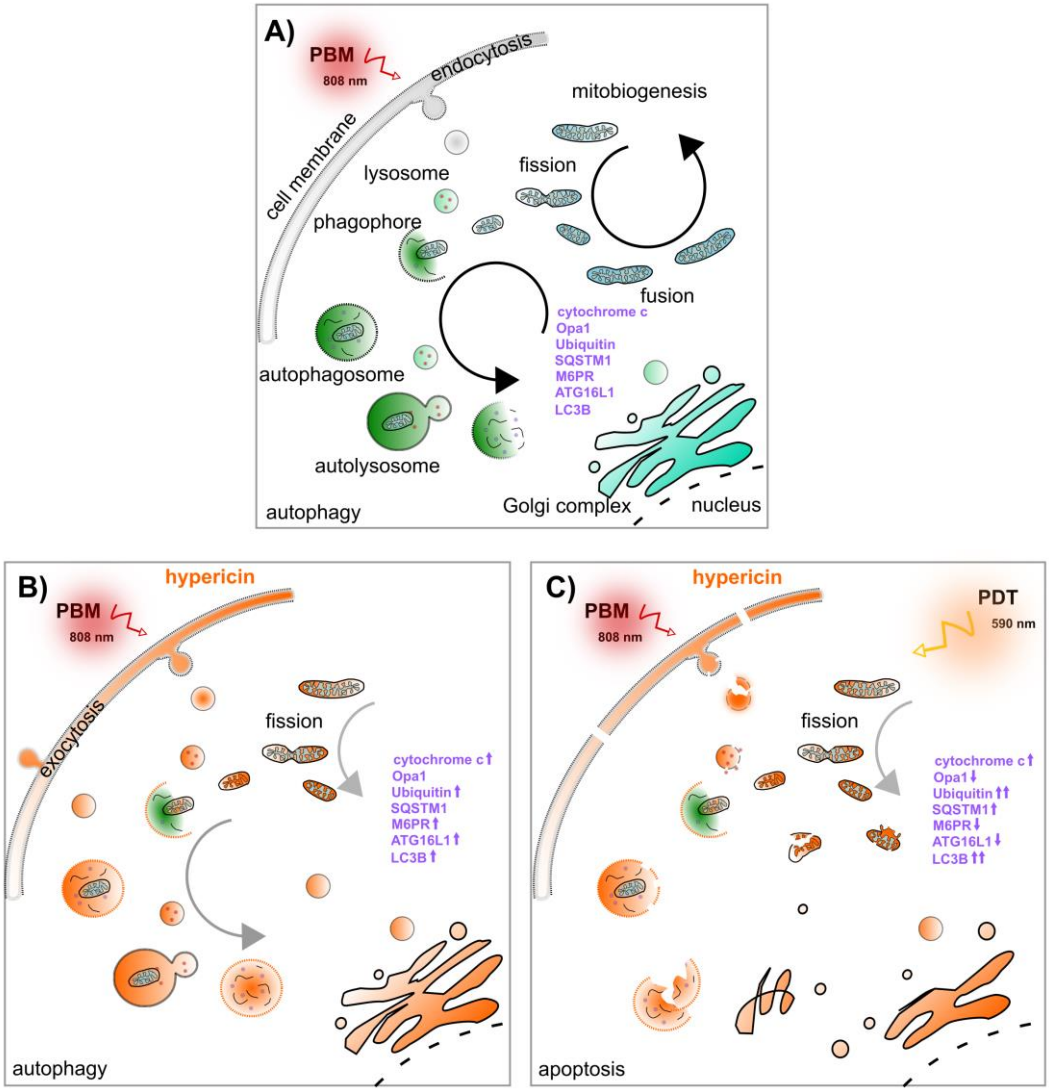

Figure 9: Schematic model of autophagy and apoptosis initiation by PBM and PDT. (A) PBM, (B) PBM+hypericin and (C) PBM+hypericin+PDT stimulation of cells, (hypericin loaded organelles are presented in orange). Elevation and reduction in protein levels of autophagic and mitochondrial protein is denoted in violet with up down arrows.

5. Conclusion

Autophagy and apoptosis are two interesting cellular signalling pathways whose mechanisms can be regulated by PBM and PDT in cancer cells. In the present study, we have shown that the combination of PBM and PDT stimulates both effects in human dermal fibroblasts. However, these effects are less pronounced in these cells than in cancer cells, which may be critical for *in vivo* treatments. Autophagic proteins have been shown to be upregulated by PBM, but autophagosome degradation was inhibited

by combination with PDT. We hypothesise that appropriate regulation of these processes by PBM could help cells escape photodestruction in healthy cells and improve treatment efficacy in cancer cells. The modulatory effect of PBM shown here might be different *in vivo* and should be investigated in further studies.

Acknowledgements

This research was funded by the Ministry of Education, Science, Research and Sport of the Slovak Republic under grant numbers VEGA 1/0156/18 and VEGA 1/0421/18, by the Slovak Research and Development Agency through the project APVV-20-0340, the Swiss National Science Foundation (project 315230 185262/1), and the European Union's Horizon 2020 research and innovation programme under grant agreement No. 952333, project CasProt (Fostering high scientific quality in protein science in Eastern Slovakia). This publication is also the result of the project implementation: Open Scientific Community for Modern Interdisciplinary Research in Medicine (acronym: OPENMED), ITMS2014+: 313011V455, supported by the Operational Programme Integrated Infrastructure, funded by ERDF.

References

[1] L.F. De Freitas, M.R. Hamblin, Proposed Mechanisms of Photobiomodulation or Low-Level Light Therapy, IEEE J. Sel. Top. Quantum Electron. 22 (2016) 348–364. https://doi.org/10.1109/JSTQE.2016.2561201.

[2] M.R. Hamblin, Mechanisms and Mitochondrial Redox Signaling in Photobiomodulation, Photochem. Photobiol. 94 (2018) 199–212. https://doi.org/10.1111/php.12864.

[3] R. Wang, Y. Dong, Y. Lu, W. Zhang, D.W. Brann, Q. Zhang, Photobiomodulation for Global Cerebral Ischemia: Targeting Mitochondrial Dynamics and Functions, Mol. Neurobiol. 56 (2019) 1852–1869. https://doi.org/10.1007/s12035-018-1191-9.

[4] I.R.C. Rocha, E. Perez-Reyes, M. Chacur, Effect of photobiomodulation on mitochondrial dynamics in peripheral nervous system in streptozotocin-induced type 1 diabetes in rats, Photochem. Photobiol. Sci. 20 (2021). https://doi.org/10.1007/s43630-021-00018-w.

[5] B.J. Quirk, H.T. Whelan, What lies at the heart of photobiomodulation: Light, cytochrome c oxidase, and nitric oxide-review of the evidence, Photobiomodulation, Photomedicine, Laser Surg. 38 (2020). https://doi.org/10.1089/photob.2020.4905.

[6] A.P. Castano, T.N. Demidova, M.R. Hamblin, Mechanisms in photodynamic therapy: Part two - Cellular signaling, cell metabolism and modes of cell death, Photodiagnosis Photodyn. Ther. 2 (2005). https://doi.org/10.1016/S1572-1000(05)00030-X.

[7] E.C. Pires Marques, F. Piccolo Lopes, I.C. Nascimento, J. Morelli, M.V. Pereira, V.M. Machado Meiken, S.L. Pinheiro, Photobiomodulation and

photodynamic therapy for the treatment of oral mucositis in patients with cancer, Photodiagnosis Photodyn. Ther. 29 (2020). https://doi.org/10.1016/j.pdpdt.2019.101621.

[8] R. Fekrazad, Photobiomodulation and Antiviral Photodynamic Therapy as a Possible Novel Approach in COVID-19 Management, Photobiomodulation, Photomedicine, Laser Surg. 38 (2020). https://doi.org/10.1089/photob.2020.4868.

[9] A.S. Garcez, M.G.T. Delgado, M. Sperandio, F.T. Dantas E Silva, J.S.R. De Assis, S.S. Suzuki, Photodynamic Therapy and Photobiomodulation on Oral Lesion in Patient with Coronavirus Disease 2019: A Case Report, Photobiomodulation, Photomedicine, Laser Surg. 39 (2021). https://doi.org/10.1089/photob.2020.4977.

[10] A. Kamuhabwa, P. Agostinis, B. Ahmed, W. Landuyt, B. Van Cleynenbreugel, H. Van Poppel, P. de Witte, Hypericin as a potential phototherapeutic agent in superficial transitional cell carcinoma of the bladder, Photochem. Photobiol. Sci. 3 (2004) 772–780. https://doi.org/10.1039/b315586b.

[11] P. Agostinis, A. Vantieghem, W. Merlevede, P.A.M. De Witte, Hypericin in cancer treatment: More light on the way, Int. J. Biochem. Cell Biol. 34 (2002) 221–241. https://doi.org/10.1016/S1357-2725(01)00126-1.

[12] X. Dong, Y. Zeng, Z. Zhang, J. Fu, L. You, Y. He, Y. Hao, Z. Gu, Z. Yu, C. Qu, X. Yin, J. Ni, L.J. Cruz, Hypericin-mediated photodynamic therapy for the treatment of cancer: A review, J. Pharm. Pharmacol. 73 (2021). https://doi.org/10.1093/jpp/rgaa018.

[13] C.D. Liu, D. Kwan, R.E. Saxton, D.W. McFadden, Hypericin and photodynamic therapy decreases human pancreatic cancer in vitro and in vivo, J. Surg. Res. 93 (2000). https://doi.org/10.1006/jsre.2000.5949.

[14] I. Zupkó, A.R. Kamuhabwa, M.A. D'Hallewin, L. Baert, P.A. De Witte, In vivo photodynamic activity of hypericin in transitional cell carcinoma bladder tumors., Int. J. Oncol. 18 (2001). https://doi.org/10.3892/ijo.18.5.1099.

[15] M. Kaleta-Richter, D. Aebisher, D. Jaworska, Z. Czuba, G. Cieślar, A. Kawczyk-Krupka, The Influence of Hypericin-Mediated Photodynamic Therapy on Interleukin-8 and -10 Secretion in Colon Cancer Cells, Integr. Cancer Ther. 19 (2020). https://doi.org/10.1177/1534735420918931.

[16] V. Huntosova, Z. Nadova, L. Dzurova, V. Jakusova, F. Sureau, P. Miskovsky, Cell death response of U87 glioma cells on hypericin photoactivation is mediated by dynamics of hypericin subcellular distribution and its aggregation in cellular organelles, Photochem. Photobiol. Sci. 11 (2012) 1428–1436. https://doi.org/10.1039/c2pp05409d.

[17] V. Pevna, G. Wagnières, V. Huntosova, Autophagy and apoptosis induced in u87 mg glioblastoma cells by hypericin-mediated photodynamic therapy can be photobiomodulated with 808 nm light, Biomedicines. 9 (2021). https://doi.org/10.3390/biomedicines9111703.

[18] C.A. Schneider, W.S. Rasband, K.W. Eliceiri, NIH Image to ImageJ: 25 years of image analysis, Nat. Methods. 9 (2012) 671–675.

https://doi.org/10.1038/nmeth.2089.

[19] J.M. Suski, M. Lebiedzinska, M. Bonora, P. Pinton, J. Duszynski, M.R. Wieckowski, Relation between mitochondrial membrane potential and ROS formation, Methods Mol. Biol. 810 (2012). https://doi.org/10.1007/978-1-61779-382-0_12.

[20] Z. Jiang, Z. Hu, L. Zeng, W. Lu, H. Zhang, T. Li, H. Xiao, The role of the Golgi apparatus in oxidative stress: Is this organelle less significant than mitochondria?, Free Radic. Biol. Med. 50 (2011). https://doi.org/10.1016/j.freeradbiomed.2011.01.011.

[21] B.B. Allan, W.E. Balch, Protein sorting by directed maturation of Golgi compartments, Science (80-.). 285 (1999). https://doi.org/10.1126/science.285.5424.63.

[22] P. Mayinger, Signaling at the Golgi, Cold Spring Harb. Perspect. Biol. 3 (2011). https://doi.org/10.1101/cshperspect.a005314.

[23] M. Misuth, J. Joniova, D. Horvath, L. Dzurova, Z. Nichtova, M. Novotova, P. Miskovsky, K. Stroffekova, V. Huntosova, The flashlights on a distinct role of protein kinase C δ: Phosphorylation of regulatory and catalytic domain upon oxidative stress in glioma cells, Cell. Signal. 34 (2017) 11–22. https://doi.org/10.1016/j.cellsig.2017.02.020.

[24] J. Zhang, Autophagy and mitophagy in cellular damage control, Redox Biol. 1 (2013). https://doi.org/10.1016/j.redox.2012.11.008.

[25] G. Ashrafi, T.L. Schwarz, The pathways of mitophagy for quality control and clearance of mitochondria, Cell Death Differ. 20 (2013). https://doi.org/10.1038/cdd.2012.81.

[26] K. Ma, G. Chen, W. Li, O. Kepp, Y. Zhu, Q. Chen, Mitophagy, Mitochondrial Homeostasis, and Cell Fate, Front. Cell Dev. Biol. 8 (2020). https://doi.org/10.3389/fcell.2020.00467.

[27] W. Wen-You Yim, N. Mizushima, Cell Discovery Lysosome biology in autophagy, Cell Discov. 6 (2020).

[28] C.M. Deus, K.F. Yambire, P.J. Oliveira, N. Raimundo, Mitochondria–Lysosome Crosstalk: From Physiology to Neurodegeneration, Trends Mol. Med. 26 (2020). https://doi.org/10.1016/j.molmed.2019.10.009.

[29] G. Bjørkøy, T. Lamark, S. Pankiv, A. Øvervatn, A. Brech, T. Johansen, Chapter 12 Monitoring Autophagic Degradation of p62/SQSTM1, Methods Enzymol. 451 (2009). https://doi.org/10.1016/S0076-6879(08)03612-4.

[30] J. Park, J. Lee, C. Choi, Mitochondrial network determines intracellular ROS dynamics and sensitivity to oxidative stress through switching inter-mitochondrial messengers, PLoS One. 6 (2011). https://doi.org/10.1371/journal.pone.0023211.